A Nanostructured Covalent Organic Framework with Readily Accessible Triphenylstibine Moieties for High-Performance Supercapacitors

Kun Kang, Zhengyi Wu, Miaomiao Zhao, Zijie Li, Yunlong Ma, Jingmin Zhang, Yan Wang, Muhammad Sajjad, Rao Tao, Li Qiu*

Yunnan Key Laboratory for Micro/Nano Materials & Technology, National Center for International Research on Photoelectric and Energy Materials, School of Materials and Energy, Yunnan University, Kunming 650091, P. R China

*Corresponding author: qiuli@ynu.edu.cn

Table of Contents

1. Materials and methods

All commercially available reagents and solvents were used as received without further purification, unless noted otherwise. NMR spectra were recorded on an Avanceiiihd-600 NMR spectrometers. Solid state cross polarization magic angle spinning (CPMAS) ^{13}CNMR spectra were recorded on an Inova 400 NMR spectrometer. The FT-IR spectra of **Sb-COF** and tris(4-formyl)antimony were obtained from Nicoletis10 FT-IR. Transmission electron microscopy (TEM) observations were done using a JEOL JEM 2100 operated at 200 kV. Scanning electron microscopy (SEM) was performed with a Carl Zeiss and Nova NanoSEM 450 microscope. The powder wide angle X-ray diffraction patterns (PXRD) were recorded on a RIGAKUTTRIII-18KW diffractometer using Cu Kα1 radiation (λ = 1.54056 Å). The XPS data was measured using the K-Alpha instrument. The BETs were obtained by temperature control with liquid nitrogen, and the pore size distribution was simulated with QSDFT (Quenched Solid Density Functional Theory). The electrical conductivity of film materials was measured by a digital four-probe tester (ST2253, Jingge Ltd. China).

2. Experimental procedures

2.1 Synthesis of tris(4-formylphenyl)antimony

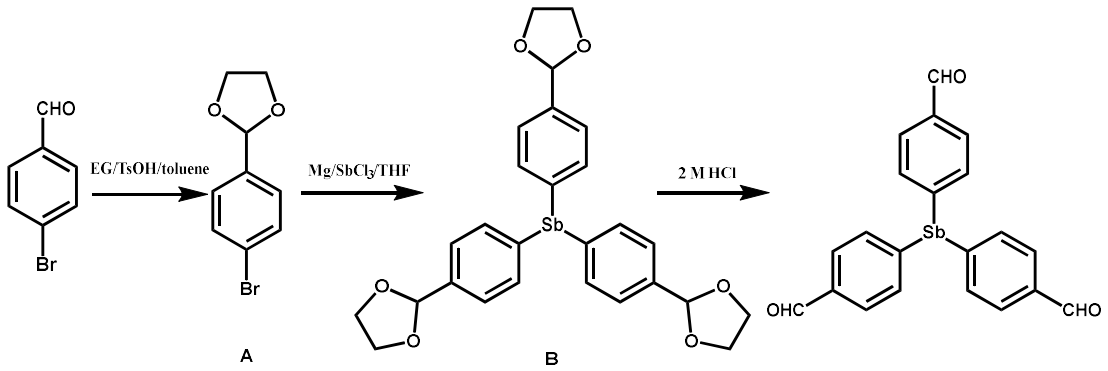

Synthesis of compound A: The mixture of p-bromobenzaldehyde (10 g, 54 mmol), ethylene glycol (33.2 ml, 59.5 mmol) and p-toluenesulfonic acid (0.9245 g, 5.37 mmol) in 90 ml of toluene were mixed well and refluxed at 110 °C for 12 h. After cooling to room temperature (r.t.), saturated $NaHCO_3$ solution was added to the reaction system before extracting with ethyl acetate (EA). The combined organic extracts were washed

with water and brine successively, dried over anhydrous Na_2SO_4. Evaporation of volatiles under vacuum gave the desired compound 2-(p-bromophenyl)dioxolane (A), which was used directly in next step.

Synthesis of compound B: Magnesium powder (700 mg, 28.81 mmol) was placed in a flask under N_2. Compound **A** (6 g, 26.2 mmol) was dissolved in 30 ml of anhydrous tetrahydrofuran (THF) and slowly added dropwise into the flask to prepare the Grignard reagent. Then $SbCl_3$ (2.03 g, 8.91 mmol) was dissolved in 10 ml of THF and slowly added dropwise to the flask before stirring at r.t. for 15 h. Saturated $NaHCO_3$ solution was added dropwise at 0 °C to quench the reaction. The resulting mixture was extracted with dichloromethane (DCM), and the combined organic extracts were washed with water and saturated brine successively, dried over anhydrous Na_2SO_4. The volatiles were removed under vacuum to give the crude product. The residue was purified by flash column chromatography using EA: PE = 4:1 as the eluent to afford the product as a white solid (9 g, 60 %).

Synthesis of tris(4-formylphenyl)antimony: Dissolve compound B into THF and add 2 M hydrochloric acid to reflux for 2 hours to remove the protecting group. $NaHCO_3$ was then added, extracted using DCM, dried over anhydrous Na_2SO_4. Evaporation of volatiles under vacuum gave the final product tris(4-formylphenyl)antimony. ^{1}HNMR ($CDCl_3$, TMS): δ (ppm) = 7.61-7.62 (6 H, m, Ar-H), 7.85-7.86 (6 H, m, Ar-H), 10.0 (3 H, s, CHO).

2.2 Synthesis of the control imine compound

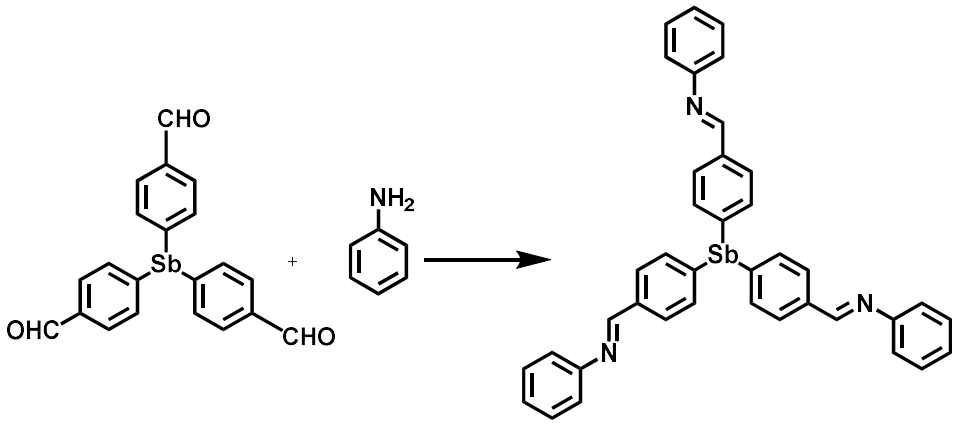

Tris(4-formylphenyl)antimony (40 mg, 0.092 mmol) was added to the solution of aniline (9.37 mg, 0.368 mmol) in 20 ml of DCM and then stirred for 24 h until the reaction was completed. A white precipitate was obtained upon addition of methanol, and the resulting solid was collected by filtration, which was washed with methanol and dried at 35 °C under vacuum overnight to yield white target product (52 mg, 85.6 %). ^{1}HNMR ($CDCl_3$) δ (ppm) = 7.21-7.24 (9 H, m, Ar-H), 7.38-7.41 (6 H, m, Ar-H), 7.58-7.59 (6 H, m, Ar-H), 7.87-7.88 (6 H, m, Ar-H), 8.46 (3 H, s, CHO).

2.3 Synthesis of Sb-COF

Sb-COF was synthesized via a solvothermal process as shown in **Figure 1a**. Tris(4-formylphenyl)antimony (40 mg, 0.092 mmol) and *p*-phenylenediamine (14.8 mg, 0.137 mmol) was dissolved in a mixed solvent system (0.28 ml of dioxane and mesitylene (v./v. = 1 : 3) in a glass tube, and then 0.18 ml of 6 M acetic acid was added. This mixture was sonicated for 15 min to obtain a homogeneous dispersion. After snap-freezing in liquid nitrogen, the glass tube was degassed by three freeze-pump-thaw cycles. Finally, the glass tube was flame-sealed in vacuum and placed at 120 °C for 72 h. After cooling to room temperature, the resulted precipitate was collected by filtration followed by Soxhlet extraction with tetrahydrofuran for 24 h, which was then dried under vacuum at 60 °C for 12 h to give the desired product as an orange solid in 72% yield. This solvothermal condensation reproducibly generates **Sb-COF** as a microcrystalline powder.

2.4 Three or two-electrode assembly

For the three-electrode system tests, COF material was employed as the working electrode, Ag/AgCl as the reference electrode, Pt mesh electrode as the counter electrode, and 1 M KOH as the electrolyte. The working electrode was prepared as follows: **Sb-COF** (70 wt%), carbon black (20 wt%), and binder (PVDF mixed with NMP) (10 wt%) in N-methylpyrrolidone (NMP) were mixed into a slurry and coated on a 1*1.5 cm^2 nickel foam. During the tests, the reference and working electrodes were

placed as closely as possible (a Luggin capillary was thus employed) to minimize the resistance caused by electrolytes and thus to weaken the voltage fluctuation. Specific capacitance (C), energy/power density (E/P), and Coulombic efficiency (η) were determined according to the following **Equations (S1-S4)**:

$$C = \frac{I \times \Delta T}{m \times \Delta V} \quad \text{(S1)}$$

$$E = \frac{1}{2} \times \frac{C \times \Delta V^2}{3.6} \quad \text{(S2)}$$

$$P = \frac{E \times 3600}{\Delta t} \quad \text{(S3)}$$

$$\eta = \frac{\Delta t}{T_c} \times 100\% \quad \text{(S4)}$$

where I is the discharge current (A), Δt is the discharge time (s), m is the mass of the active material (mg), ΔV is the charge-discharge voltage window (v), T_c is the charging time (s) during the GCD test.

2.5 Calculation of energy density for the Sb-COF//rGO ASC

Before cycling: specific capacitance = 78.6 F g^{-1} @ 3 A g^{-1}.

$$E = \frac{1}{2} \times \frac{C \times \Delta V^2}{3.6} = \frac{78.6 \times 4}{7.2} = 44 \text{ Wh Kg}^{-1}$$

After cycling (100000 cycles): specific capacitance = 124 F g^{-1} @ 3 A g^{-1}.

$$E = \frac{1}{2} \times \frac{C \times \Delta V^2}{3.6} = \frac{124 \times 4}{7.2} = 69 \text{ Wh Kg}^{-1}$$

2.6 Synthesis of amorphous triphenylstibine based porous organic polymer (Sb-POP).

The synthesis process of **Sb-POP** is the same as that of **Sb-COF**, except that the solution concentration is scaled down by a factor of 10 by using 2.8 ml instead of 0.28 ml of dioxane and 1,2,3-trimethylbenzene (v./v. = 1:3).

3. Structural characterization

3.1 Solid-State ^{13}C CP-MAS of Sb-COF

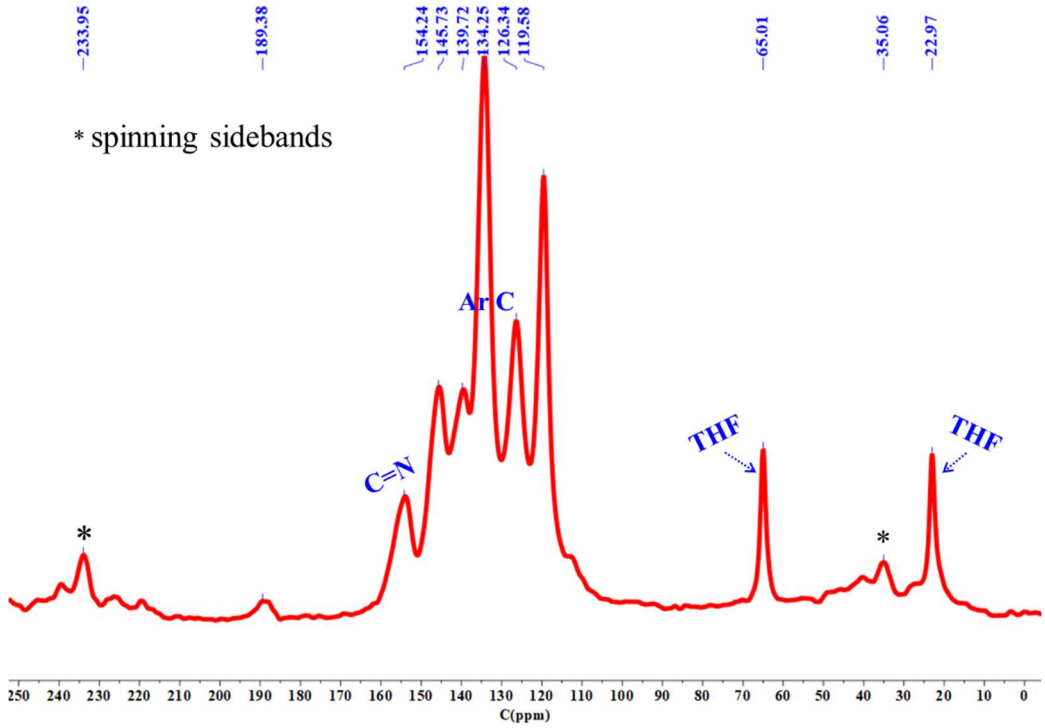

Figure S1 The solid-state ^{13}C CP-MAS NMR spectrum of **Sb-COF**. THF was left after the Soxhlet extraction.

3.2 FT-IR spectra of Sb-COF and tris(4-formylphenyl)antimony

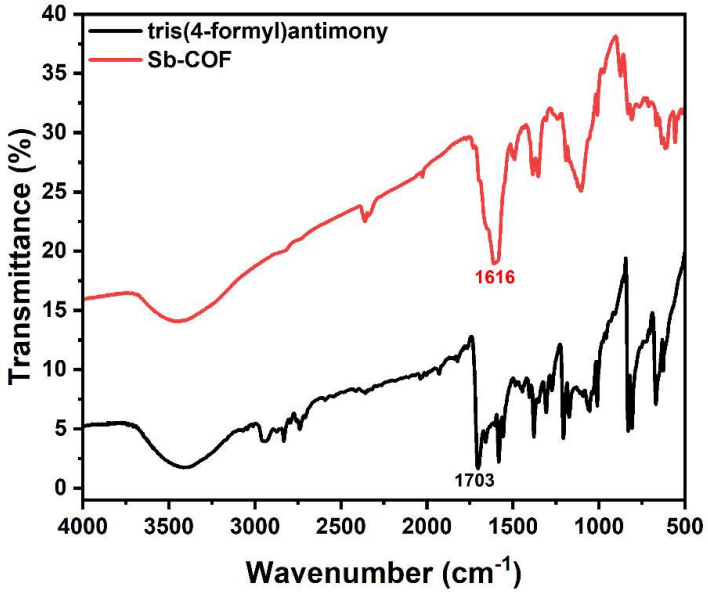

Figure S2 FT-IR spectra of **Sb-COF** and tris(4-formyl)antimony.

3.3. Structural modeling of Sb-COF

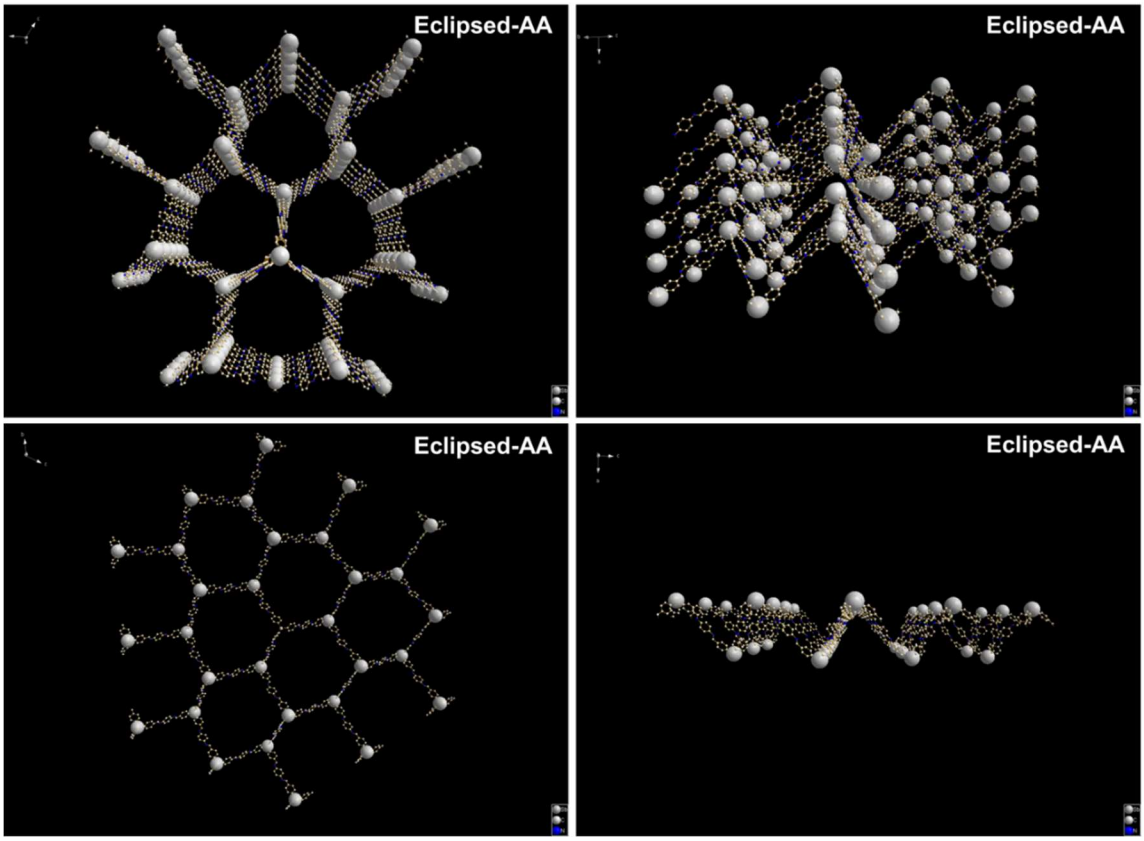

Figure S3 Top and side views of the AA stacking patterns of **Sb-COF**, as well as the structure of its monolayer molecules.

4. Supercapacitive performance of Sb-COF electrode

4.1 CV comparison of triphenylstibine and triphenylphosphine

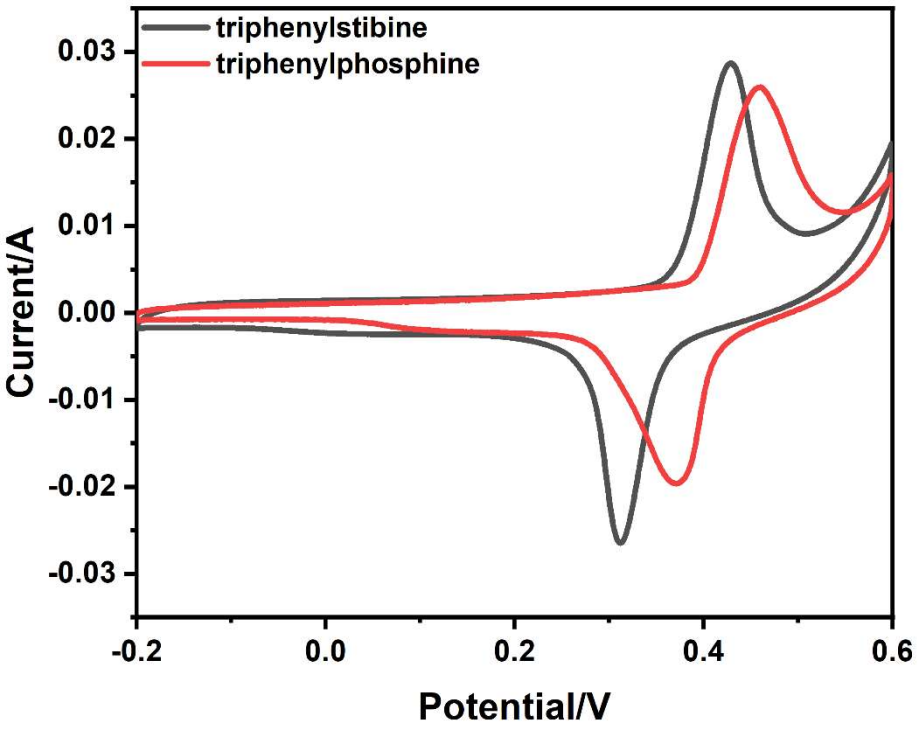

Figure S4 CV comparison of triphenylstibine and triphenylphosphine.

4.2 Electrochemical test of the control imine compound and Sb-POP

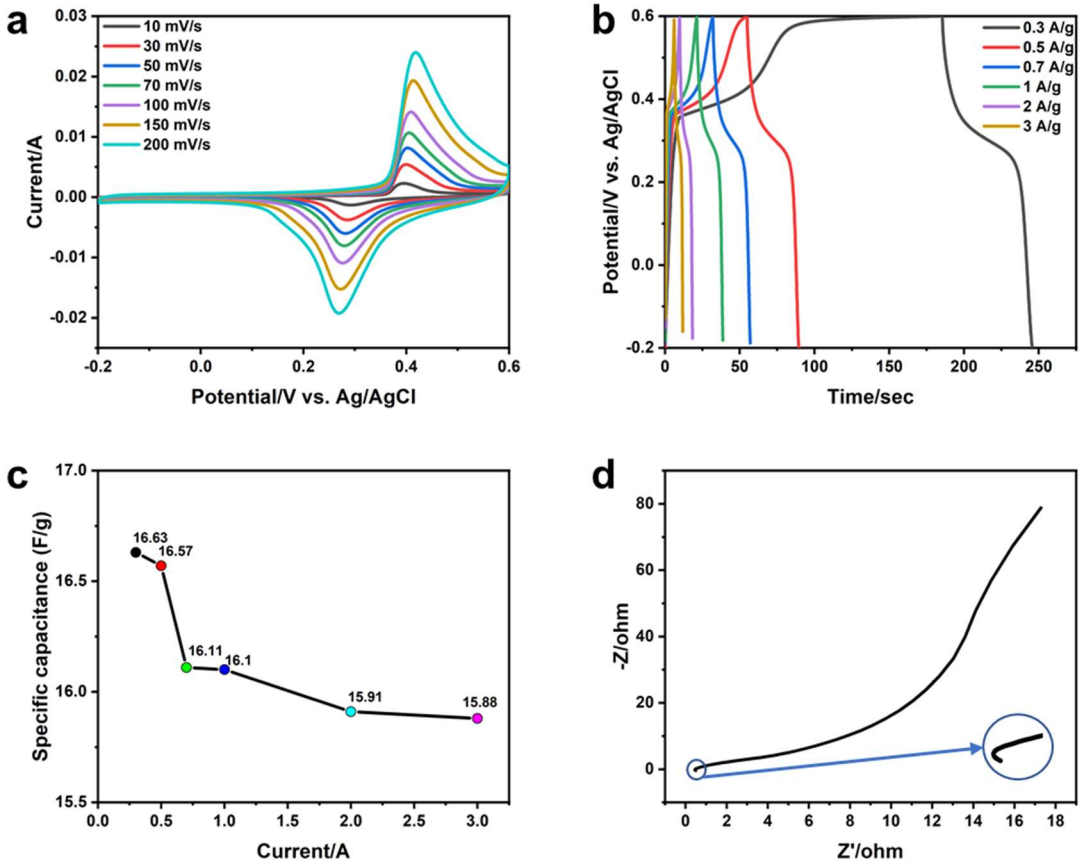

Figure S5 Electrochemical test of the control imine compound. a) CV curves at different scan rates (10~200 mV s^{-1}), b) GCD curves at different current densities (0.3~3 A g^{-1}), c) specific capacitances at corresponding current densities and d) Nyquist plots.

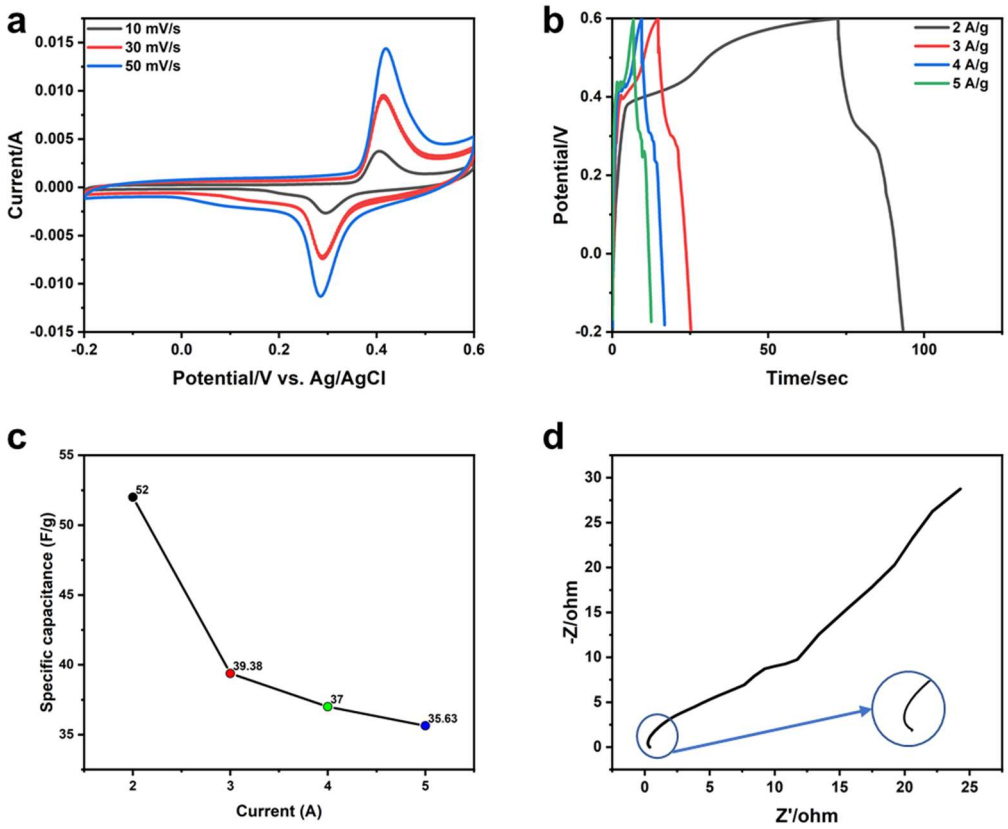

Figure S6 Electrochemical test of **Sb-POP**. a) CV curves at different scan rates (10 ~ 50 mV s^{-1}), b) GCD curves at different current densities (1 ~ 5 A g^{-1}), c) specific capacitances at corresponding current densities and d) Nyquist plots.

4.3 Calculation of diffusion coefficients

Randles-Ševčik Equation S5 was employed to calculate the diffusion coefficient of the electrolyte [1,2]:

$$i_p = 2.69 \times 10^5 n^{3/2} A C_0 D^{1/2} v^{1/2} \qquad \text{(S5)}$$

where i_p represents the peak positive current (A), n represents the number of electrons involved in the redox reaction, A represents the electrode surface area (cm^2), C_0 represents the concentration of the electrolyte (mol cm^{-3}), D represents the diffusion coefficient of the active electrode (cm^2 s^{-1}), and v presents the scan rate (V s^{-1}).

For **Sb-COF** electrode, n = 1, A = 1.5 cm^2, $C_0 = 10^{-3}$ mol cm^{-3} and i_p = 0.11 A@v = 0.1 V s^{-1}, or i_p = 0.16 A@v = 0.2 V s^{-1} (see CV curves in **Figure 3a** in the manuscript), D was calculated to be $7.66*10^{-7}$ cm^2 s^{-1}.

For **Phos-COF** electrode, n = 1, A = 1.5 cm^2, $C_0 = 10^{-3}$ mol cm^{-3} and i_p = 0.017 A@v = 0.1 V s^{-1}, or i_p = 0.029 A@v = 0.2 V s^{-1} (CV curves shown in **Figure S7**), D was calculated to be $2.18*10^{-8}$ cm^2 s^{-1}.

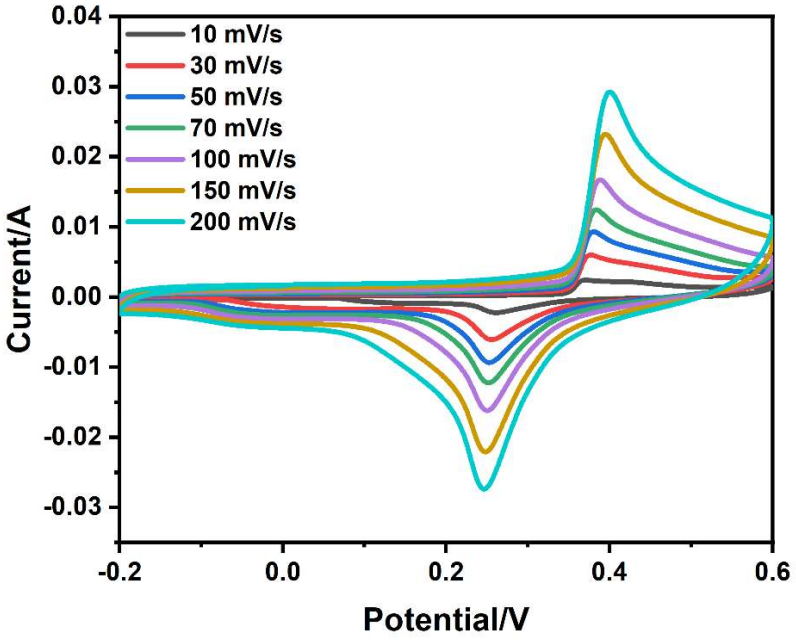

Figure S7 CV curves at different scan rates (10 ~ 200 mV s^{-1}) of Phos-COF electrode.

4.4 GCD curves for 100,000 cycling test of three electrodes

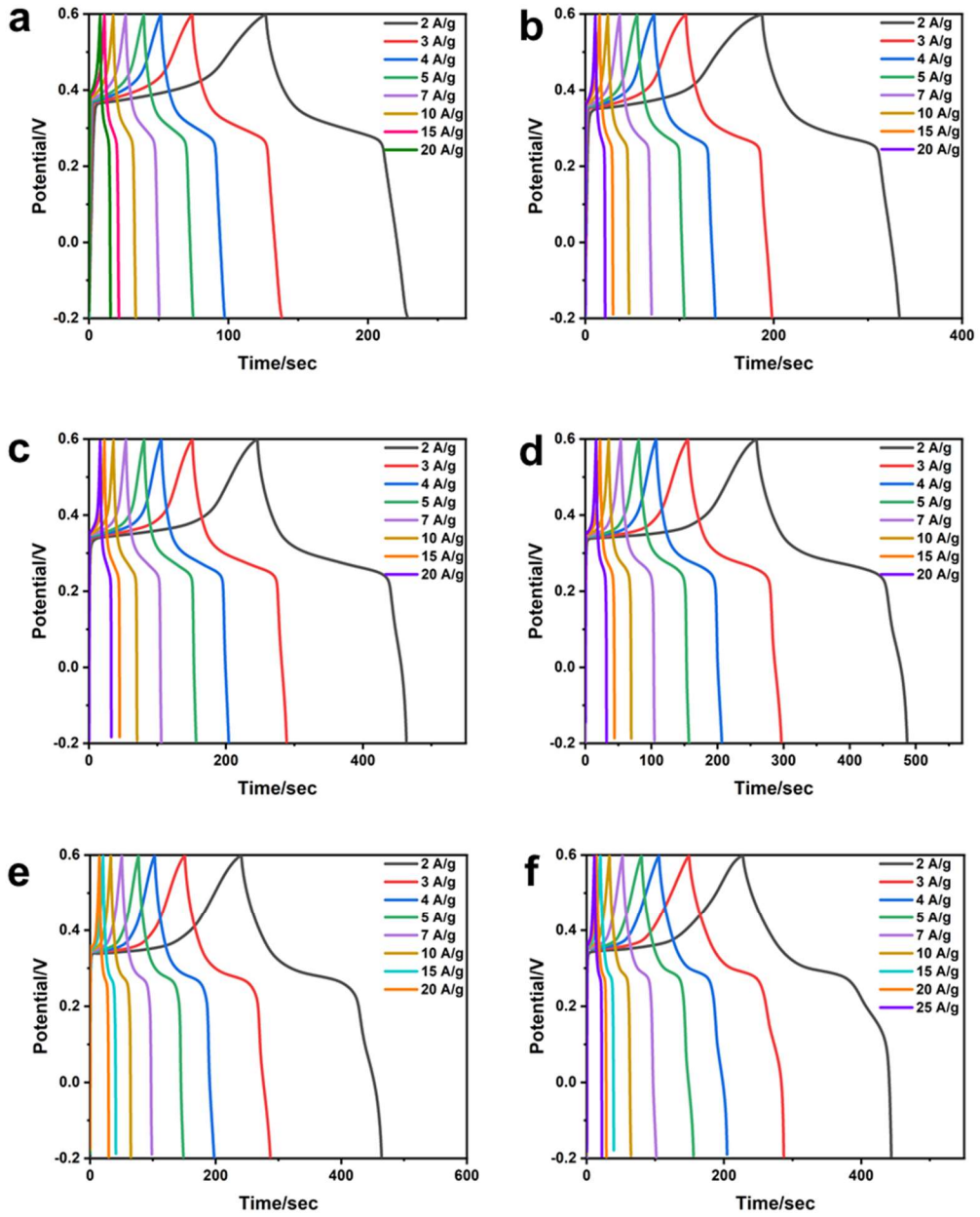

Figure S8 Real-time electrochemical test after each 20,000 cycles in a three-electrode configuration. a) Pre-Cycle, b) after 20,000 cycles, c) after 40,000 cycles, d) after 60,000 cycles, e) after 80,000 cycles and f) after 100,000 cycles.

4.5 Specific capacitances during cycling

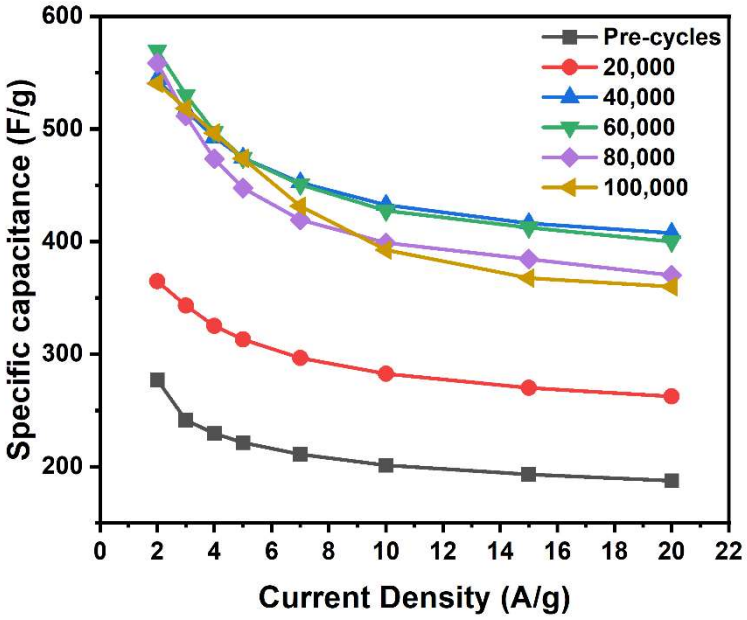

Figure S9 Specific capacitances at 2 to 20 A g^{-1} after each 20,000 cycles in a three-electrode configuration.

4.5 Electrochemical performance after 60,000 cycles

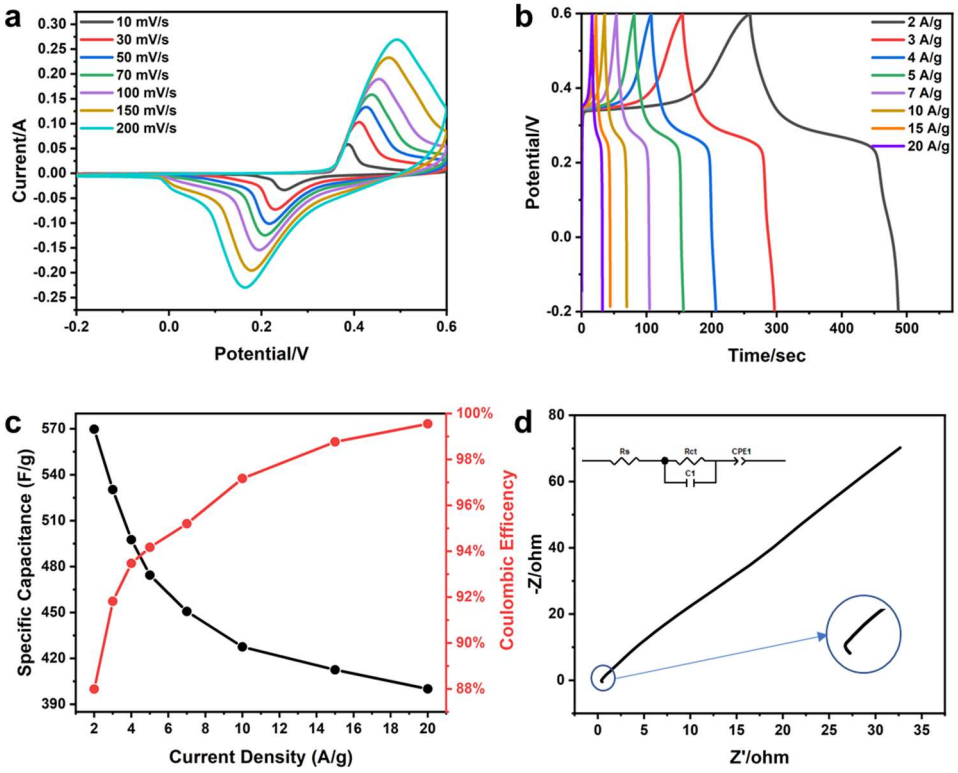

Figure S10 Electrochemical testing after 60,000 cycles. a) CV curves at different scan rates (10~200 mV s^{-1}), b) GCD curves at different current densities (2~20 A g^{-1}), and c) specific capacitance at different scan rates, d) Nyquist plots.

4.6 Diffusion control and capacitive charge at different scan rates before cycling and at 60,000 cycles

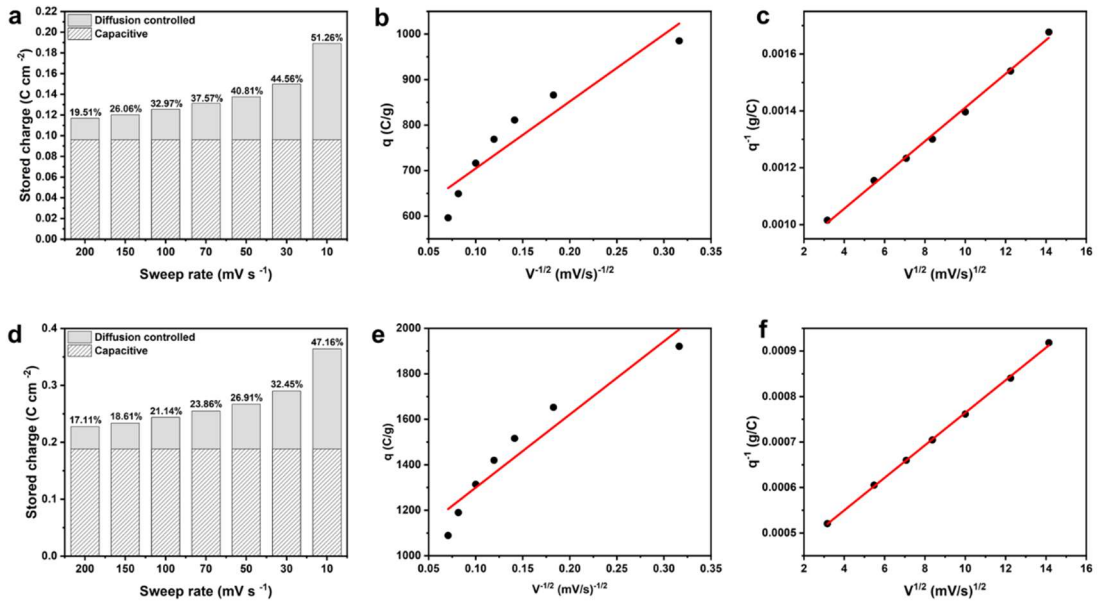

Figure S11 Analysis of diffusion-controlled and capacitive contribution of **Sb-COF** electrode in a three-electrode configuration before cycling (a~c) and after 60,000 cycles (d~f). a,d) Separation of diffusion-controlled and capacitive charge at different sweep rates, b,e) voltammetric charge (q) versus scan rate ($v^{-1/2}$) and c,f) inverse voltammetric charge versus square root of scan rate ($v^{1/2}$).

5. Determination of redox-active moieties accessed

5.1 Determination of redox-active triphenylstibine moieties accessed in a three-electrode configuration

(1) The loading mass of Sb-COF on electrode = 8 mg

Sb comprise 22.33 % of this mass

8 mg × 22.33 % = 1.786 mg of Sb occupied on electrode surface

(2) Convert the mass above to moles

$\frac{1.786\times10^{-3}\ g}{121.8\ g/mol}$ = 1.47×10^{-5} mol Sb on electrode surface

(3) Each antimony cell is a 2-electron transfer process (as proposed below), determine the number of moles of electrons

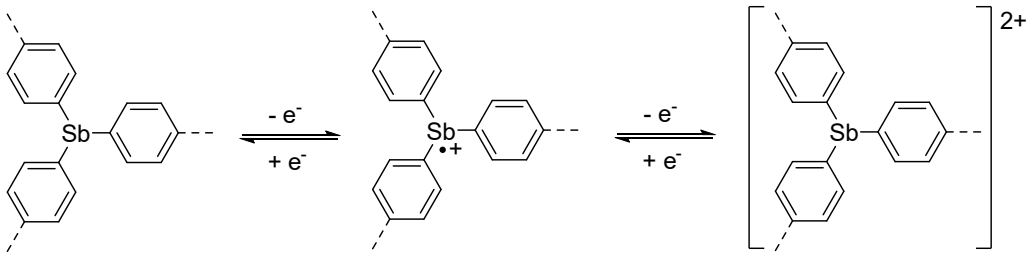

1.47×10^{-5} mol Sb $\left(\frac{2\ mol\ e^-}{mol\ e^-}\right) = 2.94 \times 10^{-5}$ e$^-$

(4) Determine the maximum coulombs of charge possible to pass

2.94×10^{-5} mol e$^-$ $\left(\frac{N_A \times 1.602 \times 10^{-19}}{mol\ e^-}\right)$ =2.84 C

(5) Integrated charge obtained from the GCD curves

Example:

(i) At current density of 20 A g^{-1}, the discharge time of working electrode is 7.5 s, 1.2 C of discharge is passed

$Q = I \times t = 20\ A/g \times 0.008 \times 7.5\ s =$ 1.2 C

(ii) And after 10,000 cycles at current density of 20 A g^{-1}, the discharge time of working electrode is 8.4 s, 1.34 C of discharge is passed

$Q = I \times t = 20\ A/g \times 0.008 \times 8.4\ s =$ 1.34 C

(iii) And after 20,000 cycles at current density of 20 A g^{-1}, the discharge time of working electrode is 10.5 s, 1.68 C of discharge is passed

$Q = I \times t = 20\ A/g \times 0.008 \times 10.5\ s =$ 1.68 C

(iv) And after 30,000 cycles at current density of 20 A g^{-1}, the discharge time of working electrode is 14 s, 2.24 C of discharge is passed

$Q = I \times t = 20\ A/g \times 0.008 \times 14\ s =$ 2.24 C

(v) And after 40,000 cycles at current density of 20 A g^{-1}, the discharge time of working electrode is 15.3 s, 2.44 C of discharge is passed

$Q = I \times t = 20\ A/g \times 0.008 \times 16.3\ s =$ 2.44 C

(vi) And after 50,000 cycles at current density of 20 A g^{-1}, the discharge time of working electrode is 15.9 s, 2.54 C of discharge is passed

$Q = I \times t = 20\ A/g \times 0.008 \times 15.9\ s =$ 2.54 C

(vii) And after 60,000 cycles at current density of 20 A g^{-1}, the discharge time of working electrode is 16 s, 2.56 C of discharge is passed

$Q = I \times t = 20\ A/g \times 0.008 \times 16\ s =$ 2.56 C

(viii) And after 70,000 cycles at current density of 20 A g^{-1}, the discharge time of working electrode is 15 s, 2.4 C of discharge is passed

$Q = I \times t = 20\ A/g \times 0.008 \times 15\ s =$ 2.4 C

(ix) And after 80,000 cycles at current density of 20 A g^{-1}, the discharge time of working electrode is 14.8 s, 2.37 C of discharge is passed

$Q = I \times t = 20\ A/g \times 0.008 \times 14.8\ s =$ 2.37 C

(x) And after 90,000 cycles at current density of 20 A g^{-1}, the discharge time of working electrode is 14.1 s, 2.26 C of discharge is passed

$Q = I \times t = 20\ A/g \times 0.008 \times 14.1\ s =$ 2.26 C

(xi) And after 100,000 cycles at current density of 20 A g^{-1}, the discharge time of working electrode is 14.3 s, 2.29 C of discharge is passed

$Q = I \times t = 20\ A/g \times 0.008 \times 14.3\ s =$ 2.29 C

(6) Divide the integrated charge by the theoretical and multiply by 100%

$\frac{1.2}{2.84} \times 100\% = 42.3\ \%$ (i)

$\frac{1.34}{2.84} \times 100\% = 47.2\ \%$ (ii)

$\frac{1.68}{2.84} \times 100\% = 59.2\ \%$ (iii)

$\frac{2.24}{2.84} \times 100\% = 78.9\ \%$ (iv)

$\frac{2.44}{2.84} \times 100\% = 85.9\ \%$ (v)

$\frac{2.54}{2.84} \times 100\% = 89.4\ \%$ (vi)

$\frac{2.56}{2.84} \times 100\% = 90.1\ \%$ (vii)

$\frac{2.4}{2.84} \times 100\% = 84.5\ \%$ (viii)

$\frac{2.37}{2.84} \times 100\% = 83.5\ \%$ (ix)

$\frac{2.26}{2.84} \times 100\% = 79.6\ \%$ (x)

$\frac{2.29}{2.84} \times 100\% = 80.6\ \%$ (xi)

5.2 Determination of redox-active triphenylphosphine moieties accessed in a three-electrode configuration

(1) The loading mass of **Phos-COF** on electrode = 8 mg

P comprise 6.1 % of this mass

8 mg × 6.1 % = 0.488 mg of P occupied on electrode surface

(2) Convert the mass above to moles

$\frac{4.88\times10^{-4}\ g}{30.97\ g/mol} = 1.57\times10^{-5}$ mol P on electrode surface

(3) Each antimony cell is a 2-electron transfer process, determine the number of moles of electrons

1.57×10^{-5} mol Sb $\left(\frac{2\ mol\ e^-}{mol\ e^-}\right) = 3.14 \times 10^{-5}$ e^-

(4) Determine the maximum coulombs of charge possible to pass

3.14×10^{-5} mol e^- $\left(\frac{N_A\times1.602\times10^{-19}}{mol\ e^-}\right)$ =3.03 C

(5) Integrated charge obtained from the GCD curves

Example:

(i) At current density of 2 A g^{-1}, the discharge time of working electrode is 22 s, 0.352 C of discharge is passed

$Q = I \times t = 2\ A/g \times 0.008 \times 22\ s =$ 0.352 C

(6) Divide the integrated charge by the theoretical and multiply by 100%

$\frac{0.352}{3.03} \times 100\% = 11.6\ \%$

5.3 Comparison of the electrode conductivity of Sb-COF and Phos-COF

Table S1. Conductivity comparison of the **Sb-COF** electrode and **Phos-COF** electrode with the same composition ratio (COF: carbon black: binder =70 wt%: 20 wt%: 10 wt%) by four-probe method.

entry	conductivity (s/cm)	
	Phos-COF	**Sb-COF**
1	0.0625	0.1667
2	0.0625	0.2222
3	0.07407	0.1
4	0.0742	0.3667
5	0.0606	0.4762
6	0.0703	0.4878
7	0.0704	0.4723
8	0.0645	0.4762
9	0.05405	0.4963
10	0.05405	0.5
11	0.06452	0.4878
12	0.05263	0.3977
13	0.07047	0.3279
14	0.08	0.3226
15	0.08696	0.1923
16	0.05	0.1942
17	0.07143	0.2817
18	0.0625	0.2778
19	0.06061	0.1942
20	0.05128	0.2817
21	0.06897	0.2778
22	0.07143	0.2532
23	0.0625	0.2633
24	0.06061	0.4369
25	0.05128	0.2554
26	0.06897	0.2987
27	0.07407	0.2778
28	0.06897	0.4762
29	0.04762	0.4878
30	0.04878	0.4369
average value	**0.064**	**0.340**

6. Supercapacitive study of Sb-COF//rGO ASC

6.1 Screening of the potential window for Sb-COF//rGO ASC

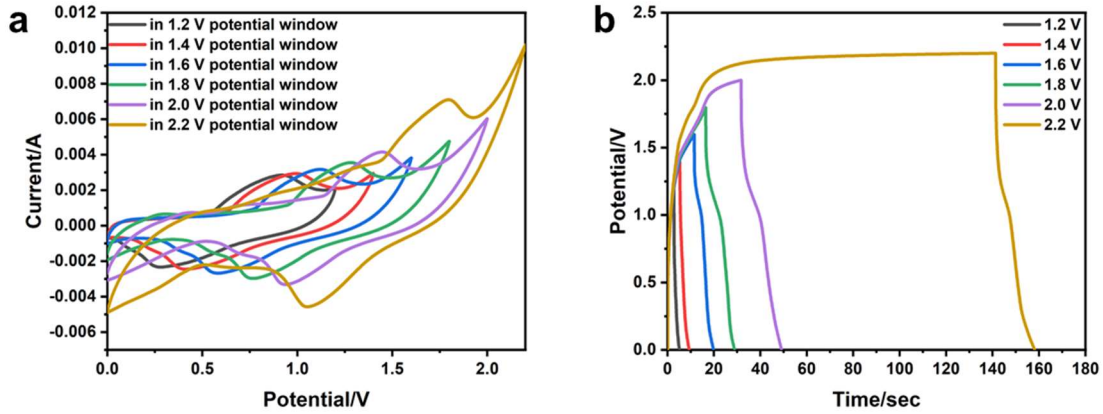

Figure S12 Potential window screen. Electrochemical characteristics of Sb-COF//rGO ASC devices, a) CV curves at 50 mV s^{-1} with various potential windows, b) GCD curves at 5 A g^{-1} with various potential windows.

6.2 Nyquist and Bode Plots Test Results Simulated from Z-View Software for the Sb-COF//rGO ASC during cycling

Table S2: Resistance analysis before and after cycling

Num. of cycles	Pre-Cycling	After-Cycling (100,000 cycles)
Rs (Ω)	23.1	21.4
R_{ct} (Ω)	4.7	4.6

7. Relevant characterization before and after cycling

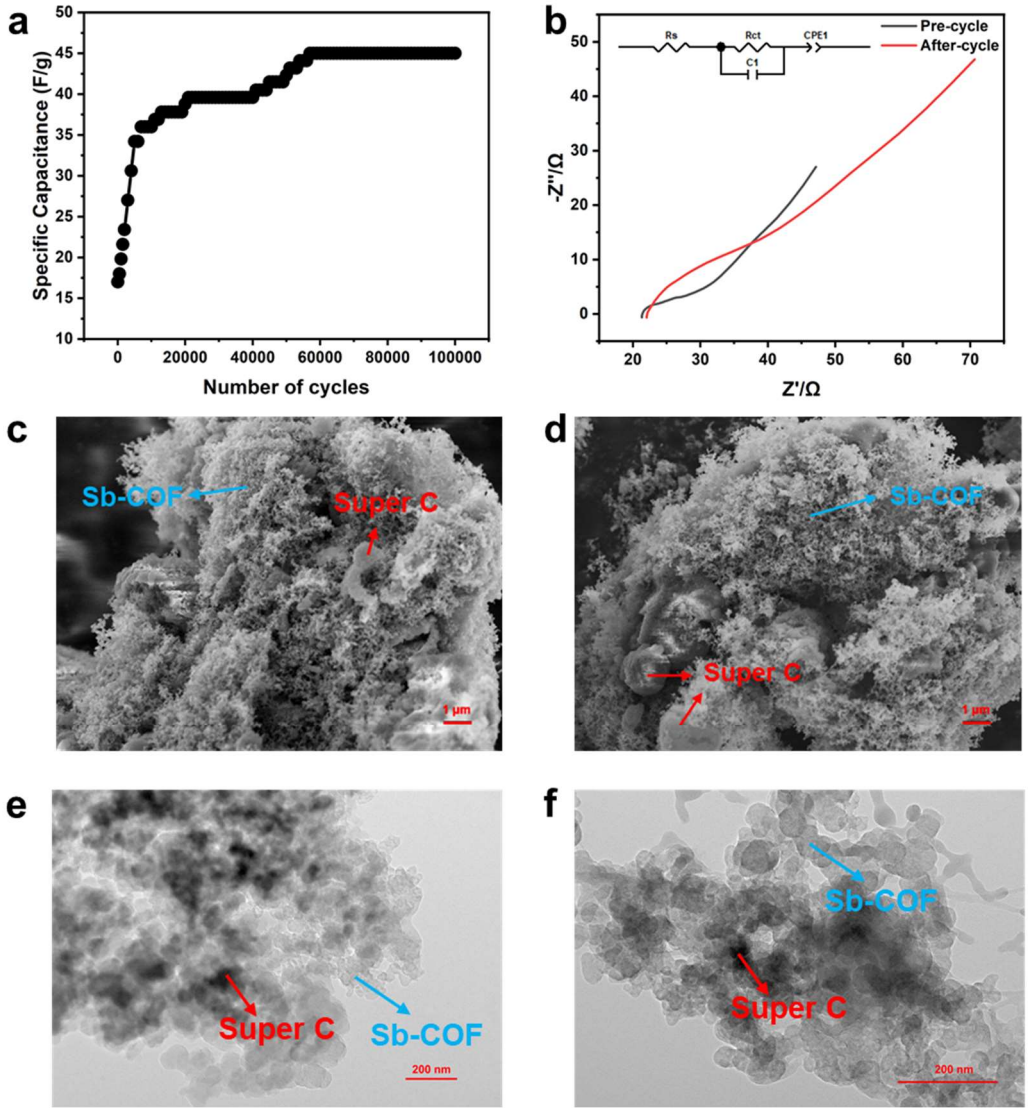

Figure S13 Electrochemical performance of Sb-COF//rGO ASC devices during the cycling test (100,000 cycles). a) The specific capacitance corresponding to the GCD cycling curve at the current density of 9 A g^{-1} (in 100,000 cycles), b) the Nyquist plot during 100,000 cycles, SEM plots c) before and d) after 100,000 cycles and TEM plots e) before and f) after 100,000 cycles.

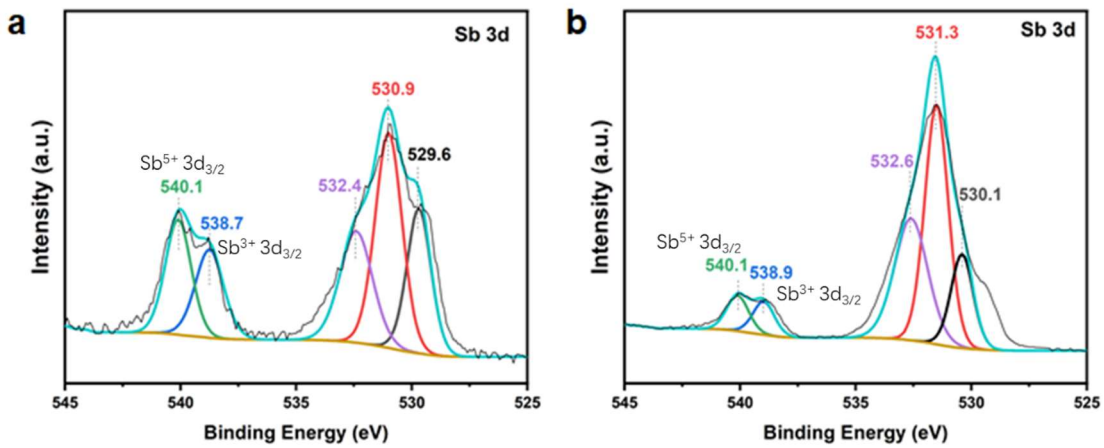

Figure S14 XPS characterization of **Sb-COF** before (a) and after (b) cycling (100,000 cycles). The Sb $3d_{3/2}$ peaks at 538.7 (538.9), and 540.1 eV are attributable to Sb^{3+} and Sb^{5+} respectively. The peak (525-535 eV) corresponding to Sb $3d_{5/2}$ states is overlapped with the O 1s peaks and it is difficult to accurately distinguish the Sb $3d_{5/2}$ peak from the O 1s region.

8. Cycling stability test of Phos-COF//rGO ASC

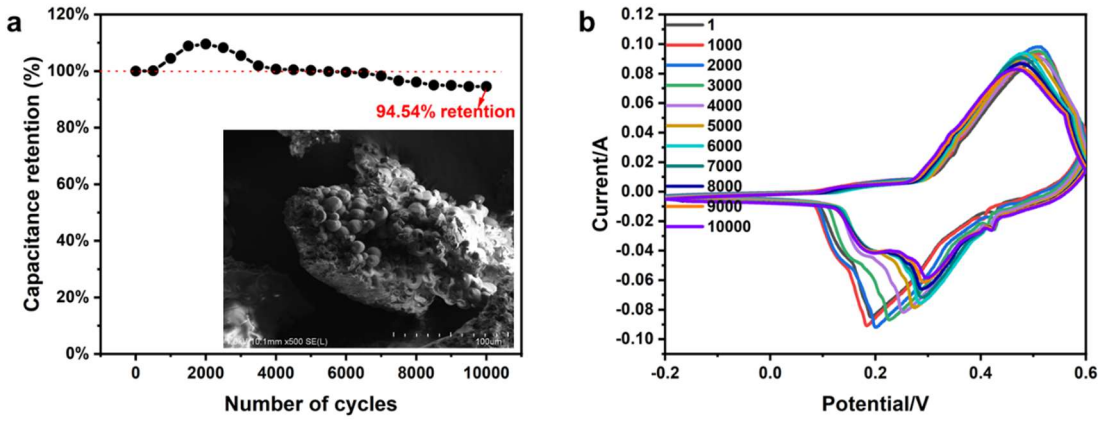

Figure S15 Electrochemical performance of Phos-COF//rGO ASC in 1 M KOH (Ag/AgCl as reference electrode, **Phos-COF** as working electrode and Pt mesh electrode as counter electrode). a) Trend graph of stability test at 50 mV s^{-1} for 10,000 cycles and SEM graph of Phos-COF at 100 μm, b) CV graph of 10,000 cycles using 50 mV s^{-1}.

9. Summarized performance of Sb-COF compared to the reported pristine COFs

Table S3. Summarized performance of Sb-COF compared to the reported pristine COFs

Electrode material	BET ($m^2 g^{-1}$)	PSD (nm)	Electrolyte	Potential window (V)		SC ($F g^{-1}$)		Energy density ($Wh kg^{-1}$)	Power density ($W kg^{-1}$)	Ref.
				Three	Two	Three	Two			
DAAQ-TFP COF	1124	2.3	1 M H_2SO_4	0.6	0.6	311	-	31	558	[3]
TpPa-$(OH)_2$-COF	369	1~1.8	1 M HPO_4	0.9	0.7	416	214	29	1956	[4]
PDC-MA-COF	748.2	1.9	6 M KOH	0.4	1.5	335	94	29.2	750	[5]
DqTp-COF	577	2~2.3	1 M H_2SO_4	1	-	111	-	0.43 $\mu Wh cm^{-2}$	980 $\mu W cm^{-2}$	[6]
TaPa-Py COF	687	1.5	1 M H_2SO_4	0.7	0.8	180.5	85.3	9.06	100	[7]
DAB-TFP COF	385	1.5	1 M H_2SO_4	0.7	0.8	98	42.7	3.8	9.06	[7]
BIBDZ	177	3.05	1 M H_3PO_4	1.0	1.0	88.4	-	12.3	249.8	[8]
DBT-MA-COF	121	1.3	6 M KOH	0.45	1.6	407	90	32.1	800	[9]
CAP-1	704	0.6	2 M KCl	1		81	-	-	-	[10]
CAP-2	594	0.7	2 M KCl	1	1.6	240	233	23	2220	[10]
TpOMe-DAQ-COF	1734	2.3	2&3 M H_2SO_4	0.8	-	169	-	-	-	[11]
NWNU-COF-1	301	1.41	6 M KOH	0.4	-	155	-	-	-	[12]
PG-BBT	507	1.88	-	0.5	1.6	729	220	69	1010	[13]
TTF-COF1	729	1.4	3 M KOH	0.5	1.5	758	183	57	858	[14]
PYDA	105	2.8	2 M H_2SO_4	0.8	-	280	-	26	4195	[15]
PYBDA	136	1.4	2 M H_2SO_4	0.8	-	410	-	40	3085	[15]
Sb-COF	**969**	**1.2**	**1 M KOH**	**0.8**	**2.0**	**540[a] (260[b])**	**124[a] (78.6[b])**	**69[a] (44[b])**	**3024**	**This work**

[a] after 100,000 cycles

[b] before cycling

10. Structural simulation and unit cell parameters/fractional atomic coordinates of AA stacking mode of Sb-COF

The Pawley refinement of the experimental PXRD was conducted by the Reflux module in the Material Studio 7.0, resulting in the cell parameters a = 7.1 Å, b = c = 26.2 Å, α = 120°, β = γ = 90° in P1 symmetry. The modelling of the COF structure was carried out in Accelrys Material Studio 7.0 software package. The simulated PXRD patterns were determined by the Reflex module, and the unit cell was optimized by Forcite module under molecular mechanics calculation using COMPASS II as the forcefield to give the relative total energy. The refinement of cell parameters and fractional atomic coordinates for Sb-COF using the AA stacking model are listed in the following Table S5.

Table S5. Refinement of cell parameters and fractional atomic coordinates for **Sb-COF** using the AA stacking model.

Sample	Sb-COF Eclipsed AA
crystal system	triclinic
Space group	P1
a	7.1 Å
b	26.2 Å
c	26.2 Å
α	120°
β	90°
γ	90°

Atom name	x	y	z
Sb1	-1.366	0.3428	-1.3494
C2	-1.2227	0.382	-1.2649
C3	-1.2521	0.4421	-1.2239
C4	-1.1409	0.4706	-1.1724
C5	-0.9993	0.4391	-1.1617
C6	-0.9747	0.3784	-1.2018
C7	-1.0866	0.35	-1.253
C8	-1.1868	0.2655	-1.3939
C9	-1.2653	0.2119	-1.4377
C10	-1.1498	0.1614	-1.4675
C11	-0.9557	0.1642	-1.4536
C12	-0.8764	0.2182	-1.4105
C13	-0.9913	0.2687	-1.3813
C14	-1.1849	0.3874	-1.3813
C15	-1.2017	0.375	-1.44
C16	-1.0737	0.4003	-1.4624
C17	-0.9278	0.438	-1.426
C18	-0.9124	0.4505	-1.3673
C19	-1.0402	0.4253	-1.345
N20	-0.7882	0.4523	-1.5029
C21	-0.7847	0.4627	-1.4487
C22	-0.2562	0.0071	-1.4921
C23	-0.3778	0.0563	-1.4656
C24	-0.5486	0.0567	-1.4933
C25	-0.5971	0.0071	-1.5481
C26	-0.4756	-0.0421	-1.5746
C27	-0.3047	-0.0425	-1.5469
N28	-0.185	-0.094	-1.5748
N29	-0.6686	0.1082	-1.4653

C30	-0.8393	0.1101	-1.4837
C31	-0.014	-0.0958	-1.5566
C32	0.1017	-0.1501	-1.5864
Sb33	0.5065	-0.3303	-1.6873
C34	0.3302	-0.2522	-1.6446
C35	0.41	-0.1984	-1.6017
C36	0.2958	-0.1476	-1.5725
C37	0.0211	-0.2043	-1.6286
C38	0.1347	-0.2552	-1.6571
C39	0.3588	-0.3719	-1.7711
C40	0.3813	-0.4329	-1.8097
C41	0.2676	-0.4624	-1.8606
C42	0.1302	-0.431	-1.873
C43	0.1124	-0.3695	-1.8353
C44	0.2269	-0.3401	-1.7848
C45	0.3249	-0.3713	-1.6517
C46	0.1667	-0.4045	-1.684
C47	0.0388	-0.4268	-1.6589
C48	0.0678	-0.4158	-1.6009
C49	0.2267	-0.3828	-1.5686
C50	0.3549	-0.3604	-1.5939
C51	-0.3455	-0.4741	-1.5161
C52	-0.4853	-0.4941	-1.492
C53	-0.6451	-0.5254	-1.526
C54	-0.6626	-0.5363	-1.5842
C55	-0.5227	-0.5162	-1.6083
C56	-0.3634	-0.4851	-1.5746
N57	-0.2232	-0.4648	-1.6004
C58	-0.0697	-0.4366	-1.5728
C59	-0.4538	-0.4361	-1.9745
C60	-0.293	-0.4677	-1.9738
C61	-0.2755	-0.5281	-2.0165
N62	-0.1529	-0.4377	-1.9283
C63	-0.0035	-0.4637	-1.9222
C64	-0.5955	0.5357	-1.0175
C65	-0.4171	0.4437	-1.0596
C66	-0.5779	0.4752	-1.0603
N67	-0.7169	0.4455	-1.1062
C68	-0.8678	0.4713	-1.1117

11. NMR spectra

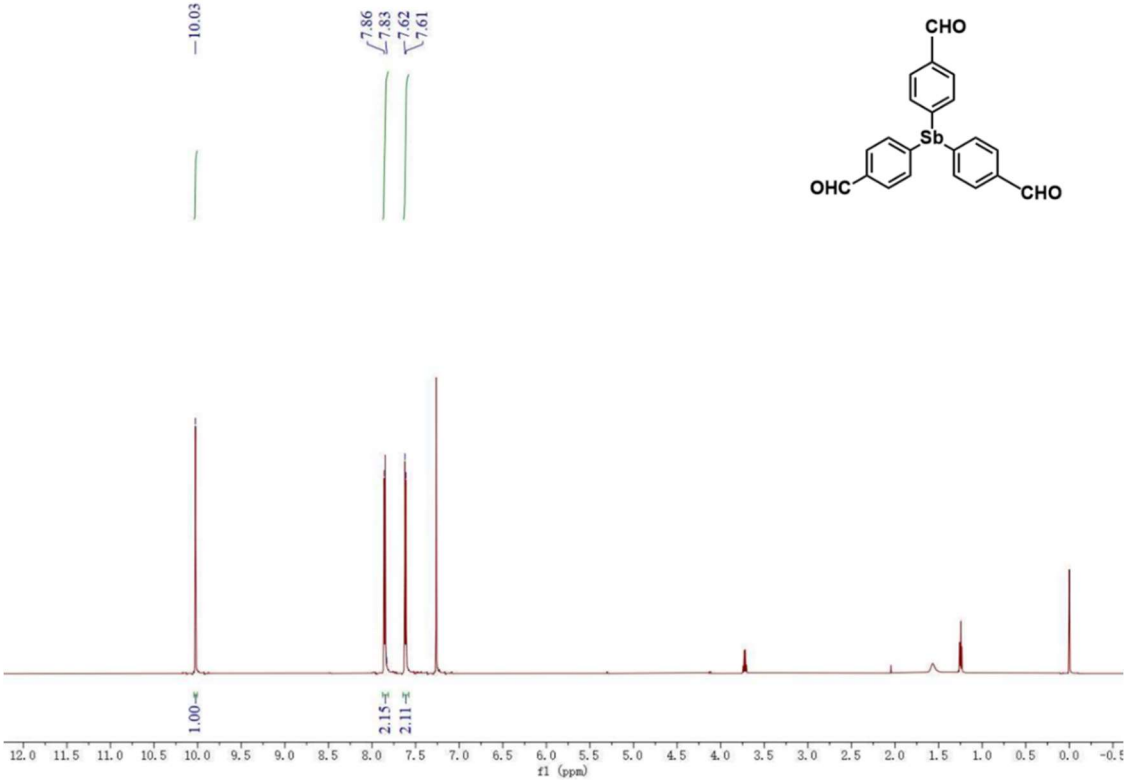

Figure S16 ^{1}H NMR of tris(4-formylphenyl)antimony

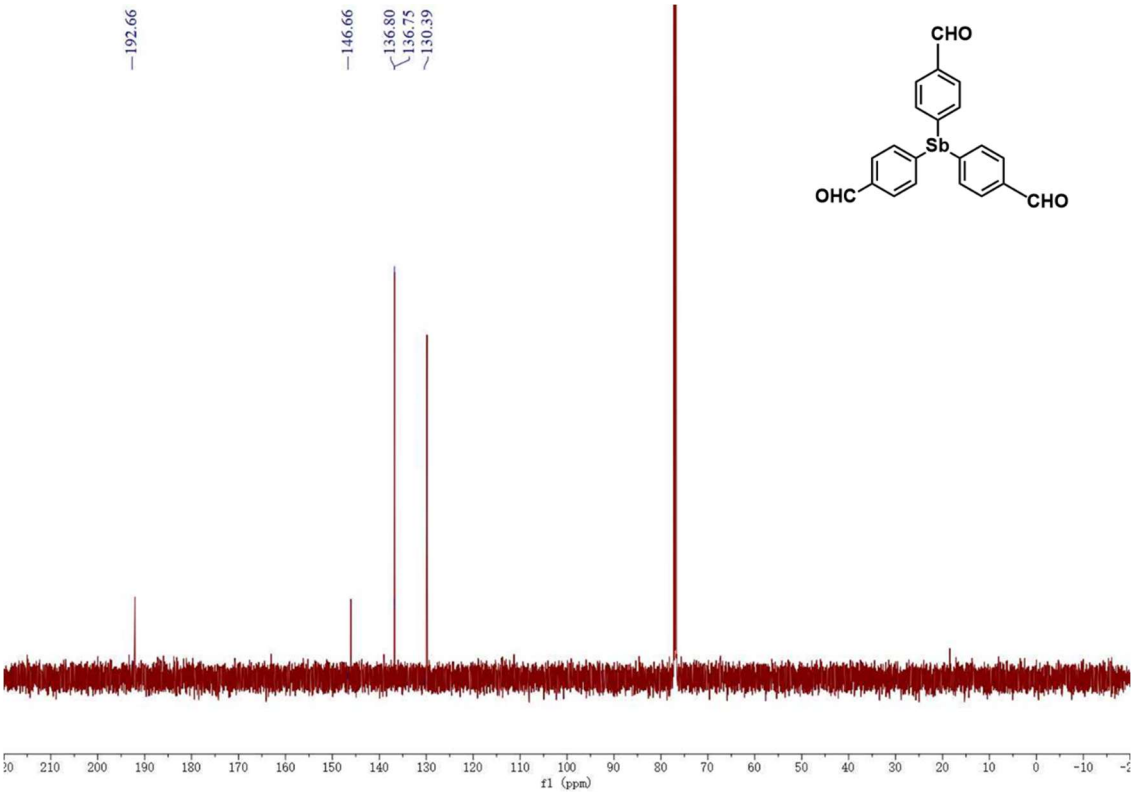

Figure S17 ^{13}C NMR of tris(4-formylphenyl)antimony

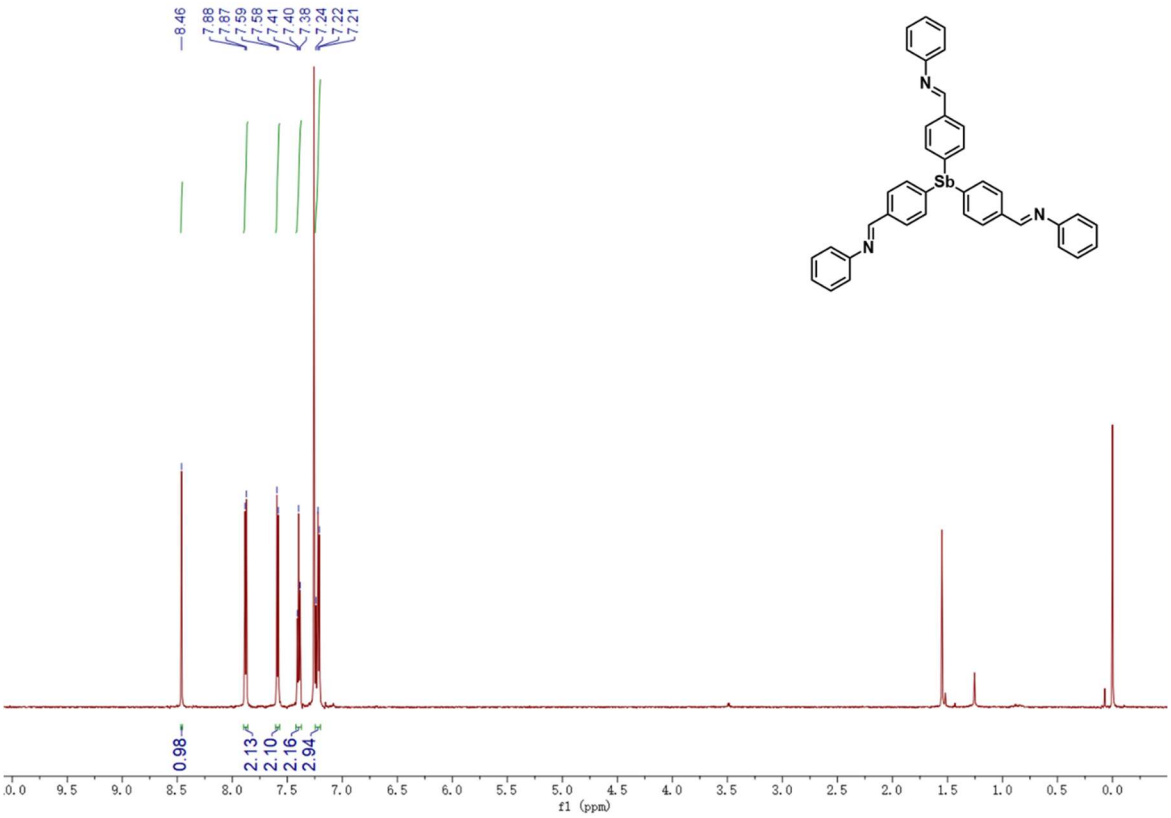

Figure S18 ^{1}H NMR of the control imine compound.

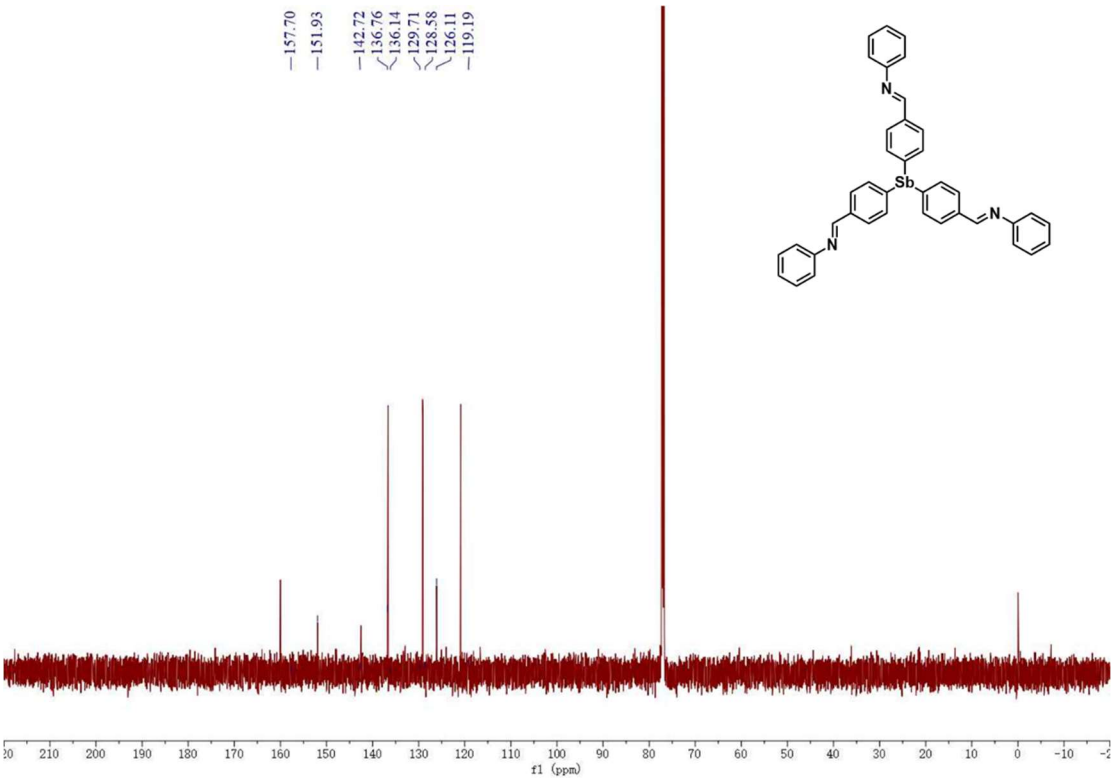

Figure S19 ^{13}C NMR of the control imine compound.

Reference

1. Elgrishi N, Rountree KJ, McCarthy BD, et al. A Practical Beginner's Guide to Cyclic Voltammetry. J Chem Educ. 2018, 95(2):197–206.
2. Sajjad M, Tao R, Qiu L. Phosphine based covalent organic framework as an advanced electrode material for electrochemical energy storage. J Mater Sci Mater Electron. 2021, 32(2):1602–1615.
3. Deblase CR, Silberstein KE, Truong TT, et al. β-Ketoenamine-Linked Covalent Organic Frameworks Capable of Pseudocapacitive Energy Storage. J Am Chem Soc. 2013, 135(45):16821–16824.
4. Chandra S, Roy Chowdhury D, Addicoat M, et al. Molecular Level Control of the Capacitance of Two-Dimensional Covalent Organic Frameworks: Role of Hydrogen Bonding in Energy Storage Materials. Chem Mater. 2017, 29(5):2074–80.
5. Li L, Lu F, Xue R, et al. Ultrastable Triazine-Based Covalent Organic Framework with an Interlayer Hydrogen Bonding for Supercapacitor Applications. ACS Appl Mater Interfaces. 2019, 11(29):26355–63.
6. Khayum MA, Vijayakumar V, Karak S, et al. Convergent Covalent Organic Framework Thin Sheets as Flexible Supercapacitor Electrodes. ACS Appl Mater Interfaces. 2018, 10(33):28139–46.
7. Khattak AM, Ghazi ZA, Liang B, et al. A redox-active 2D covalent organic framework with pyridine moieties capable of faradaic energy storage. J Mater Chem A. 2016, 4(42):16312–7.
8. Roy A, Mondal S, Halder A, et al. Benzimidazole linked arylimide based covalent organic framework as gas adsorbing and electrode materials for supercapacitor application. Eur Polym J. 2017, 93(June):448–57.
9. Li L, Lu F, Guo H, et al. A new two-dimensional covalent organic framework with intralayer hydrogen bonding as supercapacitor electrode material. Microporous Mesoporous Mater. 2021, 312:110766.
10. Liu W, Ulaganathan M, Abdelwahab I, et al. Two-Dimensional Polymer Synthesized via Solid-State Polymerization for High-Performance Supercapacitors. ACS Nano. 2018, 12(1):852–860.
11. Halder A, Ghosh M, Khayum AM, et al. Interlayer Hydrogen-Bonded Covalent Organic Frameworks as High-Performance Supercapacitors. J Am Chem Soc. 2018, 140(35):10941–10945.
12. Xue R, Guo H, Yue L, et al. Preparation and energy storage application of a long-life and high rate performance pseudocapacitive COF material linked with-NH-bonds. New J Chem. 2018, 42(16):13726–13731.
13. Li T, Yan X, Liu Y, et al. A 2D covalent organic framework involving strong intramolecular hydrogen bonds for advanced supercapacitors. Polym Chem. 2020, 11(1):47–52.
14. Li T, Yan X, Zhang W Da, et al. A 2D donor-acceptor covalent organic framework with charge transfer for supercapacitors. Chem Commun. 2020, 56(91):14187–14190.
15. Bandyopadhyay S, Singh C, Jash P, et al. Redox-active, pyrene-based pristine porous organic polymers for efficient energy storage with exceptional cyclic stability. Chem Commun. 2018, 54(50):6796–6799.